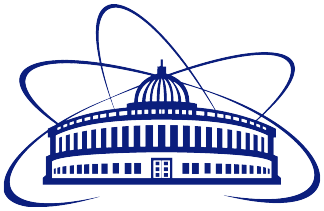

JOINT INSTITUTE FOR NUCLEAR RESEARCH
Veksler and Baldin laboratory of High Energy Physics

FINAL REPORT ON THE START PROGRAMME

Study for the Net-Proton and Net-Kaon Event-by-Event Fluctuations

Supervisor:
Dr. Vadim Kolesnikov

Student:
Rodrigo García Formentí Mendieta,
Mexico
Nuclear Sciences Institute,
National Autonomous University
of Mexico

Participation period:
July 3rd – August 25th,
Summer session, 2023

Dubna, 2023

Abstract

The properties of QCD matter in the high-baryon density domain have become a highly active research area, particularly in relation to the study of the phase diagram. In heavy-ion collisions, this is achieved by varying the collision energy and through measurements of collision energy fluctuations related to conserved quantum numbers. The net kaon measurement serves as a good proxy for the strangeness quantum number. Fluctuations in these conserved charges are quantified using high-order cumulant ratios. Specifically, the ratios C_3/C_2 and C_4/C_2 for the net kaon multiplicity have demonstrated sensitivity to the emergence of critical behavior. In this study, I developed a class for the analysis train to calculate cumulants using both reconstructed and analyzed data from Bi+Bi collisions at a center-of-center energy of $\sqrt{S_{NN}} = 9.2$ GeV, generated using the UrQMD model.

Contents

Acknowledges

I would like to express my gratitude to the Veksler and Baldin Laboratory of High Energy Physics at JINR and the START team for providing me with the opportunity to participate in the START program and to be a part of this invaluable experience.

I am sincerely thankful to my project supervisors Dr. Vadim Kolesnikov and Alexander Mudrohk. I also thank Dr. Ivonne Alicia Maldonado Cervantes, Eleazar Cuautle and Dr. Alexey Aparin for their support, guidance, and feedback throughout the project.

I finally want to thank my office mates Jorge, Nishant Santiago and Rodrigo, as well as the friends I made during the program.

Chapter 1

Introduction

Understanding the behavior of matter under extreme conditions is one of the most intriguing and fundamental quests in the realm of modern physics. The collision of heavy ions at high energies provides information for delving into the intricate dynamics of such extreme environments. While Quantum chromodynamis (QCD) has been remarkably successful in explaining the behavior of particles under normal conditions, it becomes increasingly complex when confronted with extreme temperatures and high-baryon density. The properties of QCD matter in the high-baryon density domain have become a very active field of research, particularly in relation to the study of the QCD phase diagram. The QCD critical point is a notable feature on the phase diagram. If the critical point is situated within the range accessible to heavy-ion collision experiments, it can be experimentally discovered.

The cumulants of conserved quantum numbers, such as electric charge, baryon number, or strangeness, have been shown to be sensitive indicators of critical behavior. MPD-NICA is an experiment currently in development that aims to focus on the search for the critical endpoint with heavy ions collisions in the energy range $\sqrt{S_{NN}}$ =4-11 GeV.

1.1 NICA Complex and MPD Experiment

NICA (Nuclotron-based Ion Collider fAcility) is a new particle accelerator complex designed by the JINR (Joint Institute for Nuclear Research), currently under construction in the city of Dubna, Russia. Its purpose is to experimentally study the properties of hot and dense baryonic matter, as well as spin-related properties. The main components of the NICA complex include an injection system, a booster system, a superconducting synchrotron (Nuclotron), the fixed point target experiment BM@N and a collider consisting of two superconducting rings with two interaction points: the Multi-Purpose Detector (MPD) for heavy ions and the Spin Physics Detector (SPD) for polarized proton beams. A beam transport channel is also included. The layout of the complex is illustrated schematically in Figure 1.1. As a result, the NICA ensemble encompasses three main experiments: Baryonic Matter at Nuclotron (BM@N), Spin Physics Detector (SPD), and Multi-Purpose Detector (MPD)[1]. The NICA collider will provide collisions for

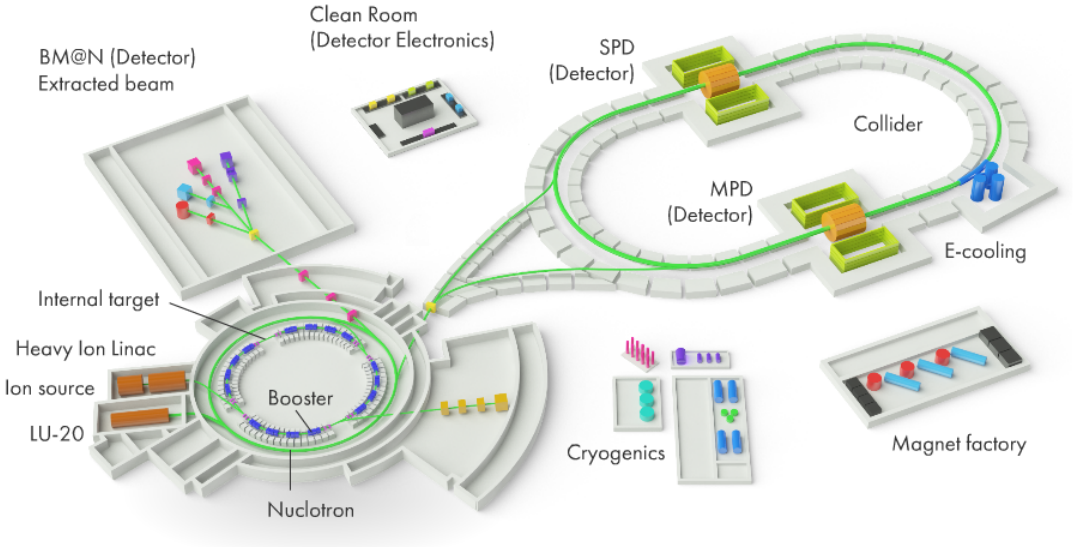

Figure 1.1: NICA Complex [2].

ions with a mass range from p to Bi, where collisions of Au ions will occur in the energy range of $\sqrt{s_{NN}} = 4 - 11$ GeV at an average luminosity of $L = 1 \times 10^{27} \text{cm}^{-2} \cdot \text{s}^{-1}$ [3].

1.1.1 Multi-Purpose Detector (MPD)

The MPD experiment is one of the three main experiments at the NICA complex, which consists of a multipurpose detector. The primary purpose of the experiment is to study the properties of hadrons, as well as the equation of state of nuclear matter, including the search for possible signals of the deconfinement phase transition and the restoration of chiral symmetry, as well as the critical point of QCD [4]. An illustration of the MPD is shown in Figure 1.2.

In the central part of the MPD, there is a Time Projection Chamber (TPC) as the main detector, surrounded by a Time-Of-Flight detector. The operation of these two detectors aims to measure momentum and identify particles. The MPD also features an Electromagnetic Calorimeter (ECal) for detecting particles such as photons and electrons, a Forward Fast Detector (FFD), and a Hadronic Calorimeter (FHCal). Other detectors will be added in subsequent phases of the experiment, such as the Inner Tracking System (ITS), which will enhance the track reconstruction process as well as the reconstruction of secondary vertices and the miniBeBe detector functions as a triggering system. To operate, the MPD is equipped with a solenoid magnet with a superconducting NbTi coil, aiming to generate a homogeneous and uniform magnetic field along the beam direction, with an intensity of up to 0.5 T.

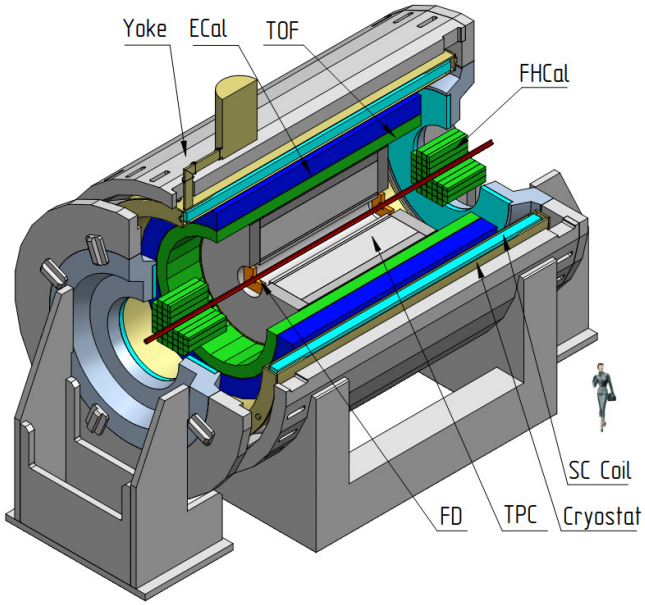

Figure 1.2: Diagram of the multipurpose detector MPD [5].

1.1.2 Time-Projection Chamber (TPC)

The TPC stands as the primary detector within the MPD, aiming to record the trajectories of charged particles and perform measurements of transverse momentum, vertex determination, and energy loss measurements (dE/dx) within the pseudorapidity range $|\eta| < 1.2$ and transverse momentum $p_t > 50$ MeV/c. The TPC assumes the form of a cylinder measuring 3.4 m in length, with an inner radius of 0.27 m and an outer radius of 1.4 m. It is filled with a gas mixture composed of 90% Ar and 10% CH_4, following the general structure of detectors used in other experiments such as the LHC and RHIC. A schematic of the TPC is depicted in Figure 1.3.

To reconstruct the trajectories of charged particles, the TPC employs a gas-filled volume with a uniform electric field. When a charged particle traverses the gas, it ionizes along its path, releasing electrons that are directed towards the detector's anode. This process yields a two-dimensional projection of the particle's track. To obtain the third component, the drift time taken by the electrons to reach the detector is measured. Applying a magnetic field allows the curvature of the track to be measured, thereby enabling the calculation of the particle's momentum. Additionally, particle identification is achieved by measuring the energy loss (dE/dx) deposited in the ionized gas. However, this method is predominantly useful in regions of low transverse momentum. The detector is designed to handle events at a maximum rate of 7 kHz.

Another characteristic of the detector lies in its ability to reconstruct primary vertices with uncertainties ranging from 150 to 700 μm in central and peripheral collisions, respectively.

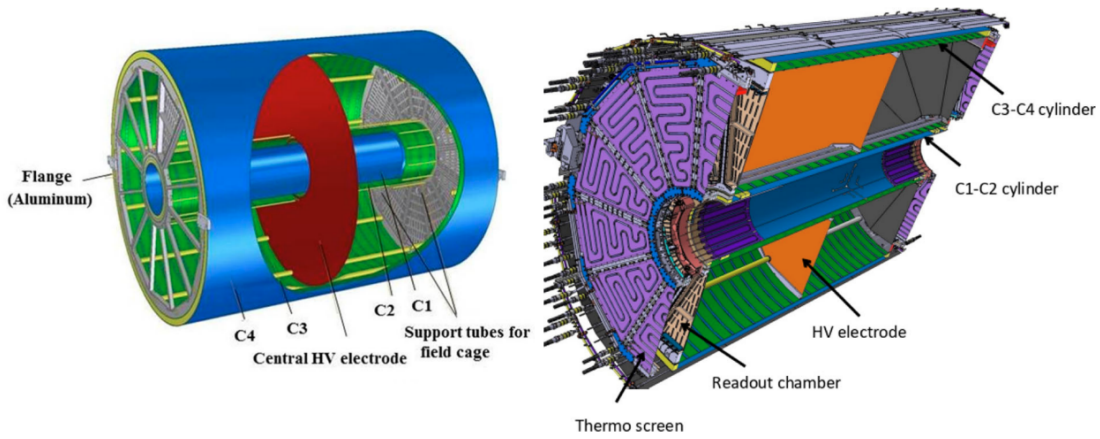

Figure 1.3: Diagram of the TPC detector with its main components [5].

1.1.3 Time-of-Flight (TOF)

The Time-Of-Flight (TOF) detector is a cylinder positioned around the TPC, with the goal of particle identification in the intermediate range of transverse momentum based on mass measurements. The TOF employs the *Multigap Resistive Plate Chambers* (MRPC) technology, which encompasses detectors filled with a gas mixture of 90% $C_2H_2F_4$, 5% SF_6, and 5% *i*-C4H10 to ascertain particle velocity with a resolution of 50 ps. A schematic of the TOF is presented in Figure 1.4.

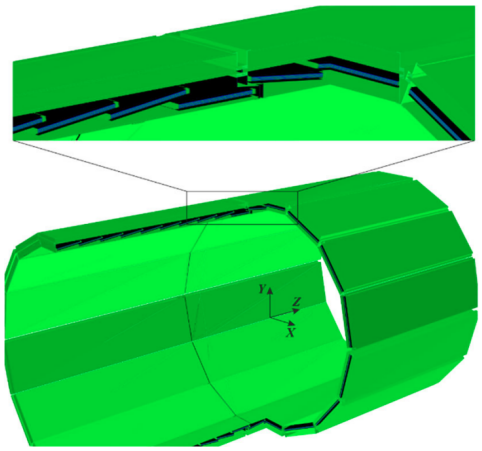

Figure 1.4: Diagram of the TOF detector with a close-up showing the MRPCs [5].

To enhance particle identification, the detected tracks from the TPC are matched with signals from the TOF. This process involves extrapolating the TPC tracks to the surface where the TOF is located and subsequently identifying the nearest signal

registered in the TOF.

1.2 Higher Moments and Cumulants

In statistics, moments are numerical measures that quantitatively depict the characteristics of a distribution. The first moment (M) yields the mean of the distribution, and the second moment (σ^2), known as the variance, is connected with the width of the distribution.
For a distribution and $n > 1$, the n^{th}-order central moment is defined as:

$$\mu_n = \mathbb{E}[(x - M)^n], \tag{1.1}$$

where M represents the mean and $\mathbb{E}$ signifies the expectation value.
The n^{th}-order normalized central moment is defined as:

$$M_n = \frac{\mathbb{E}[(x - M)^n]}{\sigma^n} = \frac{\mu_n}{\mu_2^{n/2}}, \tag{1.2}$$

where σ denotes the standard deviation.
The Skewness (S) of the distribution is defined as:

$$S = M_3 = \frac{\mu_3}{\mu_2^{3/2}} = \frac{\mathbb{E}[(x - M)^3]}{(\mathbb{E}[(x - M)^2])^{3/2}}. \tag{1.3}$$

The Skewness conveys information about the distribution's symmetry.
Lastly, the Kurtosis (κ) is defined as:

$$\kappa = M_4 - 3 = \frac{\mu_4}{\mu_2^2} - 3 = \frac{\mathbb{E}[(x - M)^4]}{(\mathbb{E}[(x - M)^2])^2} - 3. \tag{1.4}$$

The Kurtosis imparts knowledge about the probability distribution's tail and the peak of the distribution; distributions with sharper peaks have higher kurtosis. For a Gaussian distribution, both skewness and kurtosis are equal to zero.

Cumulants can be defined for a random variable X as:

$$C_n = \left.\frac{\partial^n g(t)}{\partial t^n}\right|_{t=0}. \tag{1.5}$$

Where $g(t) = \log \mathbb{E}[e^{tX}]$. These numerical values also encapsulate all the information about the distribution and share a profound connection with the moments [6].

1.3 Physics of cumulants

Let ΔN denote the net multiplicity of identified particles (in this report, focusing on kaons) within a single event, defined as $\Delta N = N - \bar{N}$ were N is the partcle multipicity

and $\bar{N}$ the antiparticle multiplicity per event. Utilizing the average net multiplicity, $\langle \Delta N \rangle$, and the deviation from its mean value, $\delta N = \Delta N - \langle \Delta N \rangle$, the initial four cumulants are defined as follows:

$$C_1 = \langle \Delta N \rangle, \quad C_2 = \langle (\delta N)^2 \rangle, \quad C_3 = \langle (\delta N)^3 \rangle, \quad C_4 = \langle (\delta N)^4 \rangle - 3\langle (\delta N)^2 \rangle^2. \tag{1.6}$$

These cumulants offer valuable insights:

$$M = C_1, \quad \sigma^2 = C_2, \quad S = \frac{C_3}{(C_2)^{3/2}}, \quad \kappa = \frac{C_4}{(C_2)^2}. \tag{1.7}$$

These parameters are interconnected with the correlation length and thermodynamic susceptibilities. Critical points are characterized by the divergence of the correlation length ξ. By utilizing QCD Lattice techniques, we establish a significant link between event-by-event fluctuation cumulants and ξ:

$$C_2 = \frac{T}{V}\xi^2, \quad C_3 = \frac{2\lambda_2 T}{V}\xi^6, \quad C_4 = \frac{6T}{V}[2(\lambda_3\xi)^2 - \lambda_4]\xi^8. \tag{1.8}$$

To eliminate volume dependency, we consider:

$$\frac{C_1}{C_2} = \frac{M}{\sigma^2}, \quad \frac{C_3}{C_2} = S\sigma, \quad \frac{C_4}{C_2} = \kappa\sigma^2. \tag{1.9}$$

Given their sensitivity to the correlation length and their connection to susceptibilities, the moments of distributions tied to conserved quantities serve as powerful tools to explore the QCD critical point and the associated phase transition [7].

Chapter 2

Methodology

To analyze the data, I developed an analysis class within the Mpdroot software framework (version 23.06.23). Mpdroot serves as a software environment for various tasks, including detector performance studies, event simulation and reconstruction, and physics analyses of both simulated and experimental data from the MPD experiment. The framework is an object orietned set of tools to simulate, transport and reconstruct MC events within MPD experiment [8].

The class I wrote is designed to work within the analysis train system. The analysis train system is a structured sequence of analysis modules meticulously crafted to process data in an organized and automated manner. Each module is tailored to address a specific analysis task, and these modules are strategically arranged to form a sequence that mirrors the logical flow of data processing.

Within my class, I utilize the Centrality wagon and the Particle Identification (PID) wagon to compute the first four cumulants of the net kaon multiplicity distribution across various centrality classes. This analysis is conducted for both the Generated Monte Carlo and the Identified particles, in the reconstruction case, the class implements a correction using factorial moments and the efficiency of the identification.

2.1 Analysed data

For the analysis, we employed the Request 25 dataset provided by the MPD collaboration, which was generated using UrQMD at a center of mass energy of $\sqrt{s_{NN}} = 9.2$ for Bi+Bi collisions. A total of 150,000 events were used for this analysis.

2.1.1 Events and tracks selection

For the 150,000 events, the following selection criteria were applied:

- z-position of collision vertex, $|V_z| \leq 100$.
- Presence of at least one charged kaon.

and for tracks selection used the next cuts:

- Number of TPC hits required for track reconstruction. $N_{hits} \geq 15$.
- Consideration of only primary tracks (MotherID).
- Transverse momentum of the track, $0.4 \leq p_T \leq 0.8$ GeV/c.
- Pseudorapidity of the primary track $|\eta| \leq 0.5$

These selection criteria are the same for the centrality and PID wagons and is preliminary and subject to optimization.

2.1.2 Kaon Identification

Particle identification within the MPD experiment relies on the Time Projection Chamber (TPC) and the Time of Flight (TOF) detector. The TPC captures ionization signals from particles as they traverse the gas volume, providing valuable insights into their momentum and energy loss. On the other hand, the TOF detector measures the time taken by particles to reach designated detectors, enabling accurate calculation of particle mass. Precise identification necessitates the fusion of information from both detectors.

In this study, I utilized the Particle Identification (PID) wagon to identify kaons. The PID wagon employs the $n\sigma$ method, utilizing parametrizations for both the TOF and TPC detectors. For this analysis, I employed both TPC$n\sigma$ and TOF$n\sigma$ variables. The resulting variables are depicted in figure 2.1.

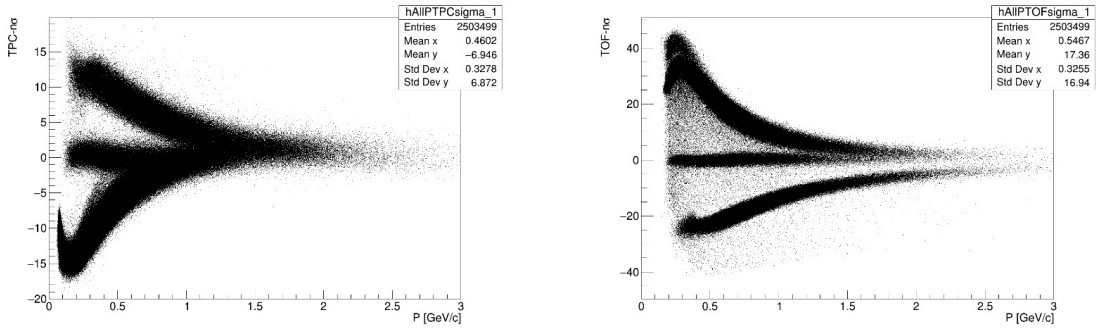

Figure 2.1: On the left side, there is a distribution of the variable TPC $n\sigma$, while on the right side, the distribution of the variable TOF $n\sigma$ is presented.

To effectively utilize TOF information, it is crucial to ensure that the track detected by TOF corresponds to the one previously identified by the TPC, thereby avoiding any potential mismatch effects. To address this concern, I implemented criteria based on $n\sigma$TOFdz and $n\sigma$TOF$d\phi$ variables that ensure that the trace detected in the TPC is the same as the one detected in the TOF. Specifically, for this analysis, tracks with $|$ $n\sigma$TOFdz $| > 2$ or $|$ $n\sigma$TOF$d\phi$ $| > 2$ were exclusively identified using the TPC (In general the tracks with this condition have a low p_T). Conversely, when these conditions were

not met, both the TPC and TOF were employed to enhance the reliability of particle identification. To identify the kaons, I made use of the following cuts

- $|n\sigma\text{TPC}(K)| < 2$ (Only TPC)
- $|n\sigma\text{TPC}(K)| < 2$ and $|n\sigma\text{TOF}(K)| < 2$ (TPC+TOF)

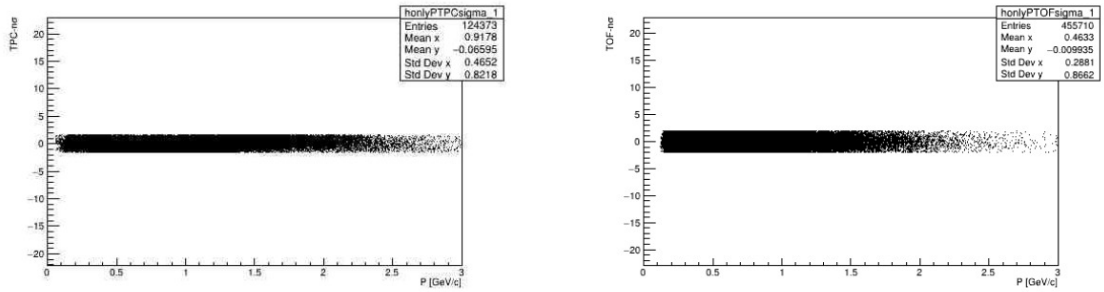

Figure 2.2: On the left side, there is a distribution of the variable TPC $n\sigma$, while on the right side, the distribution of the variable TOF $n\sigma$ is presented after cuts.

After applying these cuts, the resulting distributions of the simulated variables are depicted in Figure 2.2. Upon implementing the cuts, the efficiency of particle identification as a function of transverse momentum is displayed in Figure 2.3, while Figure 2.4 illustrates the contamination in the identification process. The efficiency distribution highlights the performance of kaon identification. Additionally, the contamination distribution showcases the degree to which other particles are erroneously identified as kaons.

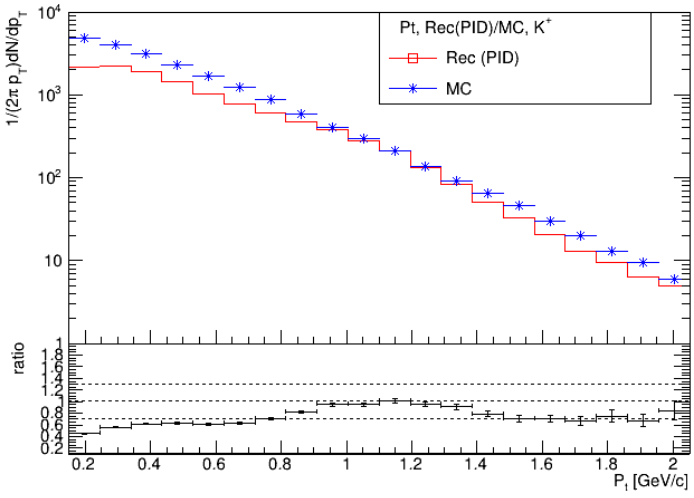

Figure 2.3: Efficiency distribution of the kaon identification.

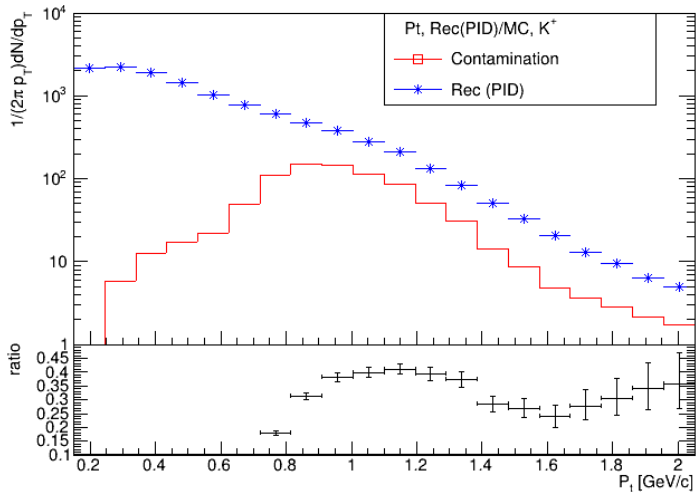

Figure 2.4: Contamination distribution for the kaon identification.

Remarkably, the contamination appears negligible within the $0.4 \leq p_T \leq 0.8$ region. However, a discernible peak of contamination becomes apparent in the range of $0.8 \leq p_T \leq 1.4$. To refine the analysis within specific p_T regions, minimizing contamination in the mid p_T interval necessitates adjustments to the identified kaon selection criteria.

Chapter 3

Net kaon Distribution Cumulants

With the particles identified, we can extract the Net kaon Distribution. The distribution for the Monte Carlo data, as well as the reconstructed and identified data, is depicted in Figure 3.1. However, in experimental measurements, only a fraction of the final-state particles can be observed. Therefore, corrections are necessary to make meaningful comparisons with theoretical calculations.

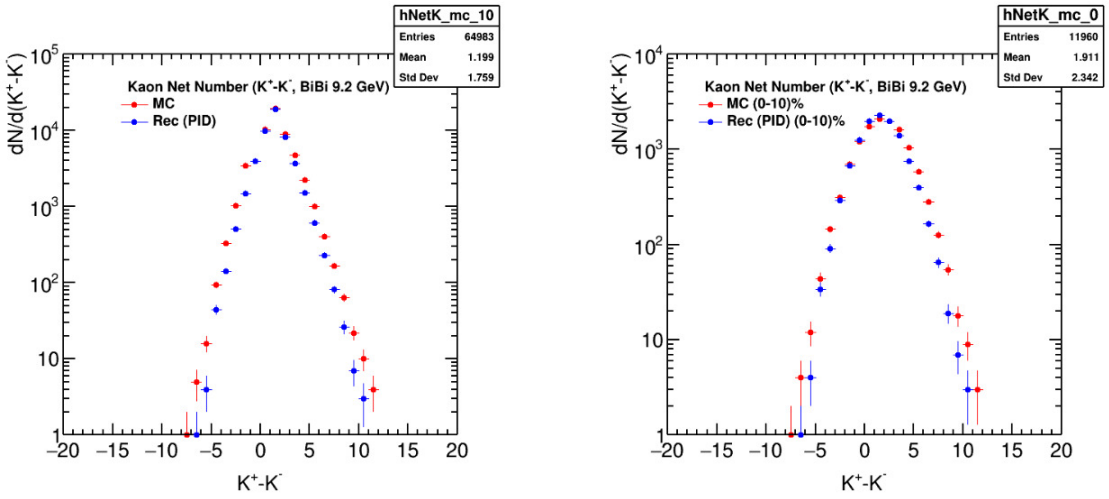

Figure 3.1: Net kaons Distribution for Monte Carlo Data and the reconstructed data. In the right side for central collisions.

3.1 Corrections with Factorial Moments

These corrections are based on the measurement of factorial moments defined as

$$f_{ik} = \left\langle \frac{n_1!}{(n_1-i)!}\frac{n_2!}{(n_2-k)!} \right\rangle = \sum_{n_1=i}\sum_{n_2=k} p(n_1,n_2)\frac{n_1!}{(n1-i)!}\frac{n_2!}{(n_2-k)!} \tag{3.1}$$

where n_1 represents the multiplicity of positive kaons, n_2 the multiplicity of negative kaons, and p denotes the detector acceptance (assuming constant acceptance independent of p_T). Assuming that acceptance corrections, like the detector efficiency and the contribution of Λ to the strangeness number, can be modeled using a binomial probability distribution, we can define

$$F_{ik} = \frac{1}{p_1^i p_2^k} f_{ik} \tag{3.2}$$

where p_1 and p_2 describes all possible acceptance effects in our system. In this context, the corrected cumulants for the identified data can be expressed as

$$\begin{aligned}
C_1 &= F_{01} - F_{02} && (3.3)\\
C_2 &= N - C_1^2 + F_{02} - 2F_{11} + F_{20} && (3.4)\\
C_3 &= C_1 + 2C_1^3 - F_{03} - 3F_{02} + 3F_{12} + 3F_{20} - 3F_{21} + F_{30} \\
&- 3C_1(N + F_{02} - 2F_{11} + F_{20}) && (3.5)\\
C_4 &= N - 6C_1^4 + F_{04} + 6F_{03} + 7F_{02} - 2F_{11} - 6F_{12} - 4F_{13} \\
&+ 7F_{20} - 6F_{21} + 6F_{22} + 6F_{30} - 4F_{31} + F_{40} \\
&+ 12C_1^2(N + F_{02} - 2F_{11} + F_{20}) - 3(N + F_{02} - 2F_{11} + F_{20})^2 \\
&- 4C_1(C_1 - F_{03} - 3F_{02} + 3F_{12} + 3F_{20} - 3F_{21} + F_{30}) && (3.6)
\end{aligned}$$

where $N = F_{10} + F_{01}$ [9]. To achieve a more accurate correction, we can calculate the efficiency of our particle identification as a function of the transverse momentum. The details of this correction procedure (used in this analysis) are described in [10].

3.2 Corrected Cumulants

To implement these corrections, it is first essential to calculate the efficiency of particle identification. This involves running the analysis twice, as the correction is applied on an event-by-event basis. Following the application of these corrections, the resulting cumulants are displayed in Figure 3.2. Additionally, Figure 3.3 presents the ratios between cumulants. These cumulant values are presented in relation to centrality classes. To delineate these classes, I employed the Centrality Wagon. The first two cumulants are higher in the central collisions, and lower in the most peripheral. The same can be said of the third cumulant. The fourth cumulant values for the first and second centrality are outside the limits of the distribution. $C_4(0-10)\% = -200. \pm 101.$ and $C_4(10-20)\% = -38 \pm 23$. These number are strange and probably due to a error in the code.

The correction made using identification efficiency and factorial moments aligns well with the Monte Carlo data. It's important to note that this correction is based on the specific Monte Carlo Generator used. In this case, I utilized UrQMD, thus similar corrections should be evaluated when employing other generators such as PHSD. The

error in the calculations is big it is purely statistical, but that's because the low statistics. It should be corrected with a larger amount of data.

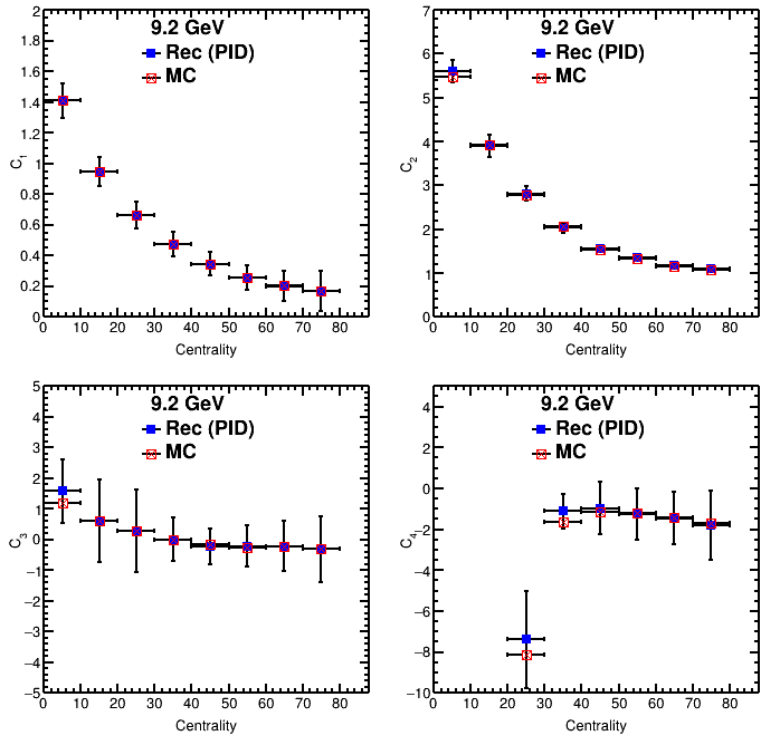

Figure 3.2: Comparison of the First Four Net kaon Cumulants in Centrality Classes: Monte Carlo vs. Identified Data

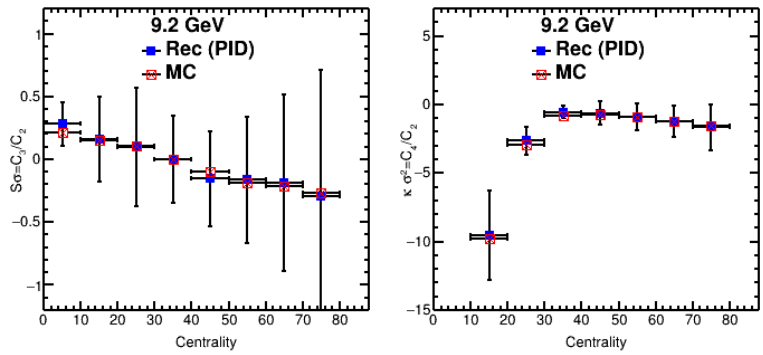

Figure 3.3: Ratios between cumulants. On the left C_3/C_2 and on the right C_4/C_2.

Chapter 4

Conclusions

The properties of QCD matter in the high-baryon density domain have become a very active field of research, particularly in relation to the study of the QCD phase diagram. In order to explore the phase diagram experimentally, the new JINR accelerator complex NICA has been designed in Dubna. The accelerator provides beams with a center of mass energy range of $\sqrt{S_{NN}} = 4 - 11GeV$. In this work, I developed a class to analyze the higher moments of the net kaon multiplicity distribution, which are directly related to the susceptibilities and correlation length in lattice QCD and have been shown to be sensitive indicators of critical behavior.

In this study, I present preliminary results of an analysis class for the MPD experiment, where I identified kaons from the reconstructed tracks to calculate the net kaon multiplicity and then the first four-order cumulants. This involves making corrections based on the calculation of factorial moments and the efficiency of identification. The macro I wrote is functional, but it is not yet optimized; further modifications are needed to optimize the particle identification and the track cuts used in the analysis. The analysis consists of two parts and is structured as two classes in the train system. The first part involves calculating the efficiency of the detector, while the second part calculates the cumulants to be used in lattice QCD calculations.

The distributions I presented originate from $150,000$ Bi+Bi collisions generated with UrQMD. The data analyzed is within the range of pseudorapidity $|\eta| \leq 0.5$, and to reduce contamination in the identification process, the transverse momentum region $0.4 \leq p_T \leq 0.8$ was considered. To identify the kaons, I made use of the PID wagon and utilized the combined TPC and TOF information. To calculate the centrality classes, I used the Centrality wagon, which employs the Glauber model. For error estimation, I utilized the factorial moments distribution, statistical errors, and propagation of uncertainty. While the cumulant correction appears effective, additional statistics are required to reduce the statistical error.

To observe the critical behavior, it is necessary to perform analyses at different energy levels. The plan is to present these distributions for various energies within the NICA collider range and subsequently compare them, while also exploring the use of alternative Monte Carlo generators. The same analytical approach can also be extended to encompass net proton multiplicity investigations.

Bibliography

[1] E. Syresin *et al.*, "NICA Accelerator Complex at JINR," in *Proc. 10th International Particle Accelerator Conference (IPAC'19), Melbourne, Australia, 19-24 May 2019*, no. 10 in International Particle Accelerator Conference, (Geneva, Switzerland), pp. 452–454, JACoW Publishing, Jun. 2019. https://doi.org/10.18429/JACoW-IPAC2019-MOPMP014.

[2] JINR, "Nica complex." `https://nica.jinr.ru/complex.php#`. 20.08.2023.

[3] M. R. Cahuantzi and for the MEXnICA group, "Mexnica, mexican group in the mpd-nica experiment at jinr," *Journal of Physics: Conference Series*, vol. 912, p. 012016, oct 2017.

[4] JINR, "The multi-purpose detector (mpd), conceptual design report." `http://mpd.jinr.ru/wp-content/uploads/2016/04/MPD_CDR_en.pdf`. 20.08.2023.

[5] T. M. Collaboration, "Status and initial physics performance studies of the MPD experiment at NICA," *The European Physical Journal A*, vol. 58, jul 2022.

[6] A. Sarkar, *Higher Moments Measurement of Net-Kaon Multiplicity Distribution in the Search for the QCD Critical Point*. Indian Institute of Thechnology, 2015.

[7] M. A. Stephanov, "Non-gaussian fluctuations near the qcd critical point," *Physical Review Letters*, vol. 102, January 2009.

[8] R. Oleg, "Purposes of the mpdroot framework." `https://mpdroot.jinr.ru/purposes-of-the-mpdroot-framework/`. 22.08.2023.

[9] A. Bzdak and V. Koch, "Acceptance corrections to net baryon and net charge cumulants," *Physical Review C*, vol. 86, oct 2012.

[10] A. Bzdak and V. Koch, "Local efficiency corrections to higher order cumulants," *Physical Review C*, vol. 91, feb 2015.